PCCP

PAPER

View Article Online
View Journal

Cite this: DOI: 10.1039/c6cp08129k

Mechanism of coverage dependent CO adsorption and dissociation on the Mo(100) surface†

Xinxin Tian,[a] Tao Wang[b] and Haijun Jiao*[c]

Received 28th November 2016,
Accepted 9th December 2016

DOI: 10.1039/c6cp08129k

www.rsc.org/pccp

The mechanism of coverage dependent CO adsorption and dissociation on the Mo(100) surface was investigated using periodic density functional theory. Structure optimization and frequency calculation were carried out using the GGA-PBE method and a $p(3 \times 3)$ supercell model. Energetic data have been obtained using the revised PBE method and the PBE optimized structures. CO adsorption prefers tilted adsorption configuration at the 4-fold hollow sites at low coverage and tilted and atop configurations at high coverage. The computed C–O stretching frequencies of the tilted and atop adsorbed CO molecules agree very well with the experimental results. Starting from the saturation coverage, five binding states have been found: two for molecular (α) CO adsorption and three for dissociative (β) CO adsorption, which are in agreement with the temperature-programmed desorption experiments. In addition, CO prefers dissociation with very low barriers in all coverages as long as free sites are available and is coverage independent; this nicely explains the observed CO dissociation at very low temperatures. All such agreements validate our computational methods and provide the basis of further studies.

1. Introduction

Carbon monoxide (CO) is one of the very important chemicals to have found wide applications in synthetic chemistry and energy in the society. Catalytic transformation is the tool in CO utilization, and understanding CO activation mechanisms can provide insights into catalytic processes, such as CO hydrogenation in Fischer–Tropsch synthesis,[1] alcohol synthesis,[2] water–gas shift reaction,[3] CO selective oxidation in fuel cells[4] and in automotive exhaust catalysts ($CO + O \rightarrow CO_2$).[5]

Since molybdenum forms very promising CO hydrogenation catalysts, such as MoS_2, Mo_2C and MoP,[6] there are numerous studies of CO adsorption on metallic molybdenum surfaces. Early ultra-high vacuum (UHV) studies focused on CO adsorption states and vibration frequencies on the single crystalline Mo(100) and Mo(110) surfaces. Using low energy electron diffraction (LEED), Auger electron spectroscopy (AES) and flash desorption spectroscopy (FDS), as well as work function measurements, Guillot *et al.*,[7,8] found both molecular (α) and dissociated (β_1, β_2, β_3) CO adsorption states on the Mo(100) surface at room temperature. Using thermal desorption spectroscopy (TDS), work function measurements and electron stimulated desorption, as well as LEED and AES, Felter and Estrup[9] studied CO adsorption on the Mo(100) surface at room temperature and at temperatures down to 200 K. They found coverage dependent desorption energies of the dissociated β state and desorption activation energy varying smoothly from an initial value of 3.7 to 2.9 eV per molecule, indicating the repulsive interaction among adjacent atoms. Using FDS, Ko and Madix[10] found chemical evidence of CO dissociation on the Mo(100) surface. Furthermore, they found that the adsorbed C and O on the Mo(100) surface strongly hinder the dissociation of CO and H_2, on the basis of LEED and AES as well as FDS, and the amount of the dissociated CO is directly related to the availability of the four-fold sites.[11] A combined study from high-resolution electron energy loss spectroscopy (HREELS), X-ray photoelectron spectroscopy (XPS) and temperature-programmed desorption (TPD) resulted in the observation of very low C–O vibration frequencies at 1065 and 1235 cm^{-1} at low coverage and temperatures below 230 K, as well as vibration frequencies at 2100 cm^{-1} at high coverage on the Mo(100) surface.[12] Using angle-resolved ultraviolet photoelectron and near-edge X-ray adsorption spectroscopies, Fulmer *et al.*,[13] found that CO exhibits vibration frequencies at 2100 cm^{-1} corresponding to CO molecules chemisorbed in atop sites at coverage higher than 50% and extraordinarily low stretching frequencies at 1200 cm^{-1} with the tilted adsorption configuration at coverage lower than 50% on the Mo(100) surface.

On the close packed Mo(110) surface, Jackson and Hooker[14] found an ordered LEED structure for CO exposure at 1273 K.

[a] *Institute of Molecular Science, Key Laboratory of Materials for Energy Conversion and Storage of Shanxi Province, Shanxi University, Taiyuan 030006, China*
[b] *Univ Lyon, Ens de Lyon, CNRS, Université Lyon 1, Laboratoire de Chimie UMR 5182, F-69342, Lyon, France*
[c] *Leibniz-Institut für Katalyse e.V. an der Universität Rostock, Albert-Einstein Strasse 29a, 18059 Rostock, Germany. E-mail: haijun.jiao@catalysis.de*

† Electronic supplementary information (ESI) available: Structures and energies IS, TS and FS of CO dissociation at each coverage (Fig. S1–S10). See DOI: 10.1039/c6cp08129k

Ericson and Estrup[15] studied CO dissociation kinetics on the clean and K-modified Mo(110) surfaces using UPS and XPS. Chen *et al.*,[16] detected CO dissociation channels on the Mo(110) surface using EELS and found that the CO species with vibration frequencies at 1345 cm^{-1} can be completely converted to C and O atoms *via* an intermediate with ν(CO) = 1130 cm^{-1}, whereas oxygen adsorption hinders CO dissociation on the surface. By applying infrared reflection absorption spectroscopy, He *et al.*,[17] studied CO adsorption on the clean and modified Mo(100) surfaces and found no vibration frequencies at 1800–2200 cm^{-1} at low CO exposure; however, they observed those vibration frequencies at exposure higher than 4 monolayers, indicating the changes of the adsorption configurations from tilted hollow sites to top sites with increasing coverage. Using high resolution core-level spectroscopy and near-edge X-ray absorption spectroscopy, Jaworowski *et al.*[18] found coverage dependent CO dissociation on the Mo(110) surface. Using a radiotracer technique, Crowell and Matthews[19] studied CO chemisorption on polycrystalline molybdenum and observed desorption at various temperatures as a function of time and a set of several binding states corresponding to desorption energies in the range of 3.24–3.95 eV.

In contrast to the plentiful experimental investigations, only few theoretical studies of CO adsorption and dissociation on Mo surfaces are available. Liu and Rodriguez[20] reported CO adsorption on the clean and modified Mo(100) surfaces and found the tilted adsorption configurations on the top site to be most stable. Ji and Li[21] computed CO adsorption and dissociation on the Mo(110) surface and found coverage dependent adsorption configurations and the hollow site to be the most stable. A barrier difference of 1 eV for CO dissociation was found between top and hollow sites. Scheijen *et al.*,[22,23] systematically calculated CO adsorption and dissociation at different coverage on the Mo(100) surface. They found that the adsorbed CO molecules up to 0.5 monolayer (ML) coverage at 4-fold hollows have the molecular axis tilted away from the surface normal by 55–57° and can dissociate easily with barriers ranging from 0.45 to 0.56 eV. On the oxygen-modified Mo(110) and (112) surfaces, Petrova[24] found that CO molecules adsorb at the hollow sites on the O/Mo(110) surface and nearly atop Mo atoms on the O/Mo(112) surface; they also observed that surface oxygen reduces the CO binding energy significantly.

Despite these experimental and theoretical studies, understanding CO interaction with Mo catalysts is far from complete. Herein, we systematically computed CO adsorption and dissociation at different coverages on the Mo(100) surface to understand the previous UHV experimental findings and rationalize coverage dependent CO adsorption and dissociation.

2. Computational methods and models

2.1 Methods

The Vienna *Ab Initio* Simulation Package (VASP)[25,26] was used for all periodic density functional theory calculations. The electron ion interaction was described with the projector augmented wave (PAW) method,[27,28] where the electron exchange and correlation energy were described by the Perdew–Burke–Ernzerhof functional within the generalized gradient approximation (GGA-PBE).[29] An energy cut-off of 400 eV and a second-order Methfessel-Paxton[30] electron smearing with σ = 0.2 eV were used to ensure accurate energies. We used the nudged elastic band (NEB)[31] method to locate the CO dissociation transition states on the surface as well as frequency analysis to verify the authentic transition state with only one imaginary frequency. Based on the PBE-optimized equilibrium structures, we further carried out single-point energies calculations using the revised PBE functional.[32] In our study, we did not include the long-range dispersion correction for van der Waals interaction because of the overestimation of the adsorption energies of strongly- and weakly-adsorbed systems.[33–35] In our studies we also found that long-range dispersion correction overestimates the CO adsorption energy on Ru(0001)[36] and the adsorption energy of H_2O on several iron surfaces.[37–39]

For coverage dependent CO adsorption, we increased the number of CO molecules one by one, *i.e.*, by adding one additional CO molecule to the previously most stable adsorption state to obtain the next most stable adsorption state by considering all adsorption sites. Herein, the stepwise adsorption energy, $\Delta E_{ads} = E_{(CO)n+1/slab} - [E_{(CO)n/slab} + E_{CO}]$, was used, where a positive ΔE_{ads} for n + 1 adsorbed CO molecules indicates the saturation adsorption with n_{CO} molecules. The CO dissociation barrier (E_a) is defined as $E_a = E_{TS} - E_{IS}$ and the reaction energy (E_r) is defined as $E_r = E_{FS} - E_{IS}$, where E_{IS}, E_{FS} and E_{TS} represent the total energy of the initial adsorbed CO molecule, final dissociated CO state (C + O atoms), and the CO dissociating transition states.

2.2 Models

Bulk optimization of body-centered cubic (bcc) Mo crystal gives a lattice constant of 3.17 Å. A $p(3 \times 3)$-5L supercell was taken to model the Mo(100) surface, where the top two layers were allowed to relax and the bottom three layers were fixed in their bulk positions. A $(5 \times 5 \times 1)$ k-point mesh was used to sample the Brillouin zone. A vacuum layer of 12 Å was set to avoid lateral slab interaction. As shown in Fig. 1, the Mo(100) has very flat surface structures with three different adsorption sites, *i.e.*, the one-fold top site (T), the two-fold bridge site (B) and the four-fold hollow site (4F).

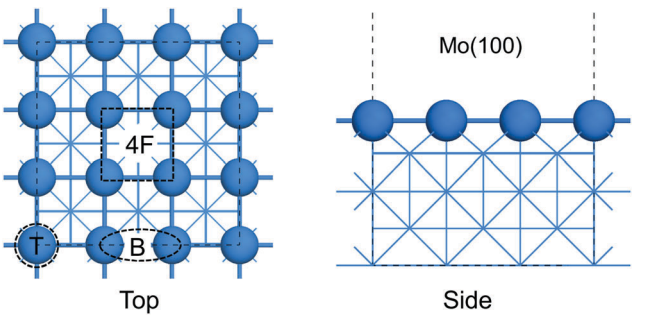

Fig. 1 Top and side views of the Mo(100) surface; and the top (T), bridge (B) and four-fold hollow (4F) adsorption sites.

3. Results and discussions

3.1 Molecular CO adsorption at different coverage

Fig. 2 shows the computed structures and stepwise adsorption energies (ΔE_{ads}) of CO adsorption at different coverage. There are three possible sites for one CO adsorption. The 4F site forms the most stable adsorption configuration with the C atom coordinating with four Mo atoms and the O atom interacting with two Mo atoms (Mo–C = 2.36 Å; Mo–O = 2.20 Å), which indicates that not only the 5σ lone pair but also the 1π bonding orbitals participate in the surface bonding.[13] The computed adsorption energy at the 4F site is −2.86 eV, which is very similar to that (−2.92 eV) computed from the observations by Scheijen *et al.*[22] Compared with the value of 1.14 Å in the gas phase, the C–O bond length is elongated to 1.37 Å with vibration frequency at 1026 cm^{-1}. This adsorption configuration corresponds to the molecular α adsorption state. Based on this most stable 4F adsorption configuration, the number of adsorbed CO molecules on the surface was further increased. To identify the most stable co-adsorption configuration at each coverage, different adsorption possibilities following the site stability order of 4F > B > T were checked. The adsorption energies of the first three CO molecules decrease slightly, indicating weak lateral repulsive interaction, whereas those of the additional CO molecules become more prominent at higher coverage, although all adsorbed CO molecules are located at the 4F sites (n_{CO} = 1–6). At $n_{CO} \geq 7$, both top and 4F adsorption configurations coexist on the surface. The saturation coverage is reached at 10 CO since a positive value of ΔE_{ads} (+0.01 eV) is found at n_{CO} = 11.

In addition, we computed CO vibration frequencies. As shown in Table 1, vibration frequencies of CO molecules at the 4F sites at coverage up to n_{CO} = 6 are in the range of 1143–1103 cm^{-1}. At higher coverage up to saturation, n_{CO} = 6–10, vibration frequencies of CO molecules at the 4F sites are in the range of 1286–1005 cm^{-1} and those of CO molecules at the top sites are in the range of 2052–1975 cm^{-1}. Early HREELS study of CO adsorption on the Mo(100) surface[12] at low temperature detected CO vibration frequencies at 1065–1235 and 2100 cm^{-1}. This agreement between theory and experiment verifies our identified adsorption configurations at different coverage and provides the rational basis for further discussions. However, the experimental results showed that CO dissociation on the Mo(100) surface became very facile at elevated temperature. In this respect, we considered the coverage dependent CO dissociation to explain the experimental findings.

3.2 CO dissociation at different coverage

Scheijen *et al.*,[22] considered the coverage dependent CO dissociation by reducing the surface slab size instead of using large slab size for more CO molecules. They also did not consider the competitive CO desorption and dissociation at different coverage. Based on the identified most stable molecular adsorption configurations at different coverage, we calculated CO stepwise dissociation. All energetic data for CO dissociation are listed in Table 2 and the structures of initial states (IS), transition states (TS) and final states (FS) are given in the ESI.† Since there are numerous possibilities at high CO coverage, the dissociation for all adsorbed CO molecules was calculated to find the energetically most favored one. For example, with *n*CO on the surface, the Mo surface has $(n - 1)$ adsorbed CO molecules and 1C + 1O after the first CO dissociation. The dissociation barrier of all the remaining $(n - 1)$ adsorbed CO molecules was considered to find the next most favorable one with $(n - 2)$ adsorbed CO molecules and 2C + 2O. The procedure was repeated until either CO desorption became more favorable than dissociation or no free sites were available for next dissociation, where the final adsorption state can be identified.

At n_{CO} = 1 (1/9 ML), the computed CO dissociation barrier is 0.58 eV, much lower than the desorption energy (2.86 eV), and

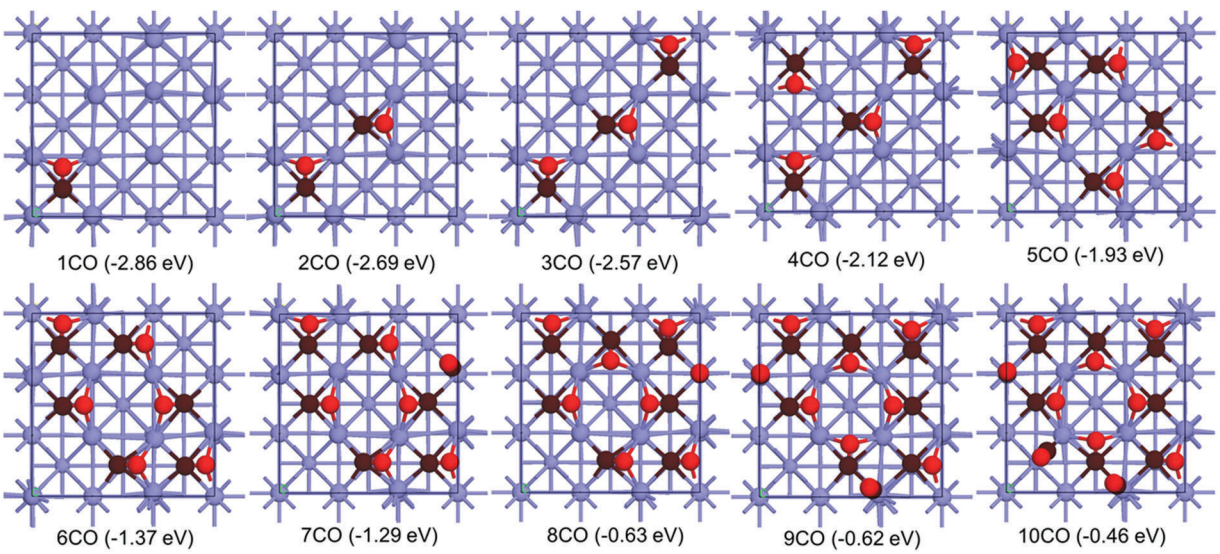

Fig. 2 Structures and energies (RPBE, ΔE_{ads}) of the most stable adsorption configuration of stepwise CO adsorption at different coverage on the Mo(100) surface (black ball for C, red ball for O and the other balls for Mo atoms).

Table 1 CO vibrational frequencies (PBE, cm^{-1}) at different coverage on the Mo(100) surface

*n*CO	Top	4F
1CO		1026
2CO		1031–1011
3CO		1020–1000
4CO		1034–1004
5CO		1055–1007
6CO		1143–1003
7CO	1975	1145–1005
8CO	2019	1162–1035
9CO	2035–2018	1131–1021
10CO	2042–1996	1139–1052
Experiment	2100	1235–1065

this process is exothermic by 1.11 eV, indicating that CO dissociation is favored kinetically and thermodynamically, and the final state has the co-adsorbed C + O atoms. At n_{CO} = 2 (2/9 ML), the barriers of the stepwise dissociation (0.52 and 0.62 eV) also are much lower than the stepwise desorption energies (2.69 and 2.59 eV), and CO stepwise dissociation is exothermic (−1.01 and −1.08 eV, respectively). Both CO molecules prefer dissociation kinetically and thermodynamically, and the final state has the co-adsorbed 2C + 2O atoms. At n_{CO} = 3 (1/3 ML), the barriers (0.48, 0.50 and 0.57 eV) of the stepwise dissociation are lower than the stepwise desorption energies (2.57, 2.56 and 2.62 eV), and CO stepwise dissociation is exothermic by 1.24, 1.11 and 0.83 eV, respectively. The final state has the co-adsorbed 3C + 3O atoms.

At n_{CO} = 4 (4/9 ML), the coverage dependent CO adsorption, with the increase of the adsorbed surface C and O atoms become evident. For example, the barriers (0.42, 0.53, 0.56 and 0.68 eV) of the stepwise dissociation are lower than stepwise desorption energies (2.12, 1.90, 1.92 and 1.65 eV), and CO dissociation is exothermic by 1.37, 0.50, 0.87 and 0.75 eV, respectively. The final state has co-adsorbed 4C + 4O atoms. With the increased number of surface C and O atoms, CO desorption energies become smaller and CO dissociation energies become less exothermic.

At n_{CO} = 5 (5/9 ML), the barriers (0.54, 0.55, 0.55 and 0.89 eV) of the stepwise dissociation of the first four CO molecules are lower than their stepwise desorption energies (1.93, 1.97, 1.85 and 1.70 eV) and their dissociation is exothermic by 1.13, 0.64, 0.64 and 0.66 eV, respectively. However, there are no free sites for the dissociation of the fifth CO molecule on the surface and the final adsorption state has one adsorbed CO molecule as well as four C and four O atoms on the surface (1CO + 4C + 4O).

At n_{CO} = 6 (2/3 ML), the dissociation barriers of the first three CO molecules (0.54, 0.52 and 0.66 eV) are lower than their stepwise desorption energies (1.37, 1.41 and 1.12 eV), and their dissociation is exothermic by 0.59, 0.54 and 0.48 eV, respectively. At this coverage, the final adsorption state has three adsorbed CO molecules as well as three C and three O atoms on the surface (3CO + 3C + 3O). Similar co-adsorption has been found at n_{CO} = 7 (7/9 ML), and the final state has four adsorbed CO molecules as well as three C and three O atoms on the surface (4CO + 3C + 3O).

At n_{CO} = 8–10 (8/9–10/9 ML), the CO desorption energies are close to the CO dissociation barriers, but CO dissociation is exothermic. This indicates that CO dissociation and desorption can form an equilibrium; however, thermodynamically, the final adsorption state has the co-adsorbed 6CO + 2C + 2O, 8CO + 1C + O and 9CO + 1C + O, respectively, for n_{CO} = 8, 9 and 10.

These systematic calculations for CO dissociation at different coverage show that CO prefers dissociation at all coverage

Table 2 Coverage dependent CO step desorption energies (ΔE_{des}, eV), and dissociation barriers (E_a, eV) as well as dissociation energies (ΔE_{dis}, eV) using RPBE functional

$n \times$ CO	ΔE_{des}	$1CO(g) + (x-1)CO + yC + yO \leftarrow xCO + yC + yO \rightarrow (x-1)CO + (y+1)C + (y+1)O$	E_a	ΔE_{dis}
1CO (1/9 ML)	2.86	1CO(g) ← **1CO** → 1C + 1O	0.58	−1.11
2CO (2/9 ML)	2.69	1CO(g) + 1CO ← **2CO** → 1CO + 1C + 1O	0.52	−1.01
	2.59	1CO(g) + 1C + 1O ← **1CO + 1C + 1O** → 2C + 2O	0.62	−1.08
3CO (1/3 ML)	2.57	1CO(g) + 2CO ← **3CO** → 2CO + 1C + 1O	0.48	−1.24
	2.56	1CO(g) + 1CO + 1C + 1O ← **2CO + 1C + 1O** → 1CO + 2C + 2O	0.50	−1.11
	2.62	1CO(g) + 2C + 2O ← **1CO + 2C + 2O** → 3C + 3O	0.57	−0.83
4CO (4/9 ML)	2.12	1CO(g) +3CO ← **4CO** → 3CO + 1C + 1O	0.42	−1.37
	1.90	1CO(g) +2CO + 1C + 1O ← **3CO + 1C + 1O** → 2CO + 2C + 2O	0.53	−0.50
	1.92	1CO(g) +1CO + 2C + 2O ← **2CO + 2C + 2O** → 1CO + 3C + 3O	0.56	−0.87
	1.65	1CO(g) + 3C + 3O ← **1CO + 3C + 3O** → 4C + 4O	0.68	−0.75
5CO (5/9 ML)	1.93	1CO(g) + 4CO ← **5CO** → 4CO + 1C + 1O	0.54	−1.13
	1.97	1CO(g) + 3CO + 1C + 1O ← **4CO + 1C + 1O** → 3CO + 2C + 2O	0.55	−0.64
	1.85	1CO(g) + 2CO + 2C + 2O ← **3CO + 2C + 2O** → 2CO + 3C + 3O	0.55	−0.64
	1.70	1CO(g) + 1CO + 3C + 3O ← **2CO + 3C + 3O** → 1CO + 4C + 4O	0.89	−0.66
6CO (2/3 ML)	1.37	1CO(g) + 5CO ← **6CO** → 5CO + 1C + 1O	0.54	−0.59
	1.41	1CO(g) + 4CO + 1C + 1O ← **5CO + 1C + 1O** → 4CO + 2C + 2O	0.52	−0.54
	1.12	1CO(g) + 3CO + 2C + 2O ← **4CO + 2C + 2O** → 3CO + 3C + 3O	0.66	−0.48
7CO (7/9 ML)	1.29	1CO(g) + 6CO ← **7CO** → 6CO + 1C + 1O	0.54	−0.61
	1.31	1CO(g) + 5CO + 1C + 1O ← **6CO + 1C + 1O** → 5CO + 2C + 2O	0.53	−0.76
	1.31	1CO(g) + 4CO + 2C + 2O ← **5CO + 2C + 2O** → 4CO + 3C + 3O	0.69	−0.50
8CO (8/9 ML)	0.63	1CO(g) + 7CO ← **8CO** → 7CO + 1C + 1O	0.67	−0.49
	0.51	1CO(g) + 6CO + 1C + 1O ← **7CO + 1C + 1O** → 6CO + 2C + 2O	0.71	−0.80
9CO (1 ML)	0.62	1CO(g) + 2CO + 1C + 1O ← **9CO** → 8CO + 1C + 1O	0.56	−0.63
10CO (10/9 ML)	0.46	1CO(g) + 9CO ← **10CO** → 9CO + 1C + 1O	0.55	−0.81

as long as free adsorption sites are available. Full CO dissociation is found at n_{CO} = 1–4 (1/9–4/9 ML), whereas molecular and dissociative adsorptions are preferred at n_{CO} = 5–7 (5/9–7/9 ML). At n_{CO} = 8–10 (8/9–10/9 ML), CO desorption and molecular adsorption as well as dissociative adsorption are possible. Most importantly, in contrast to Fe,[40–42] Co[43] and Mo_2C[44,45] surfaces, CO dissociation barriers on the Mo(100) surface are very low up to saturation coverage as long as free sites are available. This indicates a very competitive and favored CO dissociative adsorption on the Mo(100) surface as well as the very high activity of the Mo catalyst in CO dissociation. This is in line with the finding of Belosudov *et al.*,[46] *i.e.*, Mo can promote CO activation in Fe- and Co-based FTS reactions.

3.3. CO dissociation from saturation coverage

As CO desorption and molecular as well as dissociative adsorption can occur and form equilibrium at n_{CO} = 8–10, CO dissociation has a very low barrier up to saturation coverage as long as there are free sites available; we are interested in CO competitive desorption and dissociation starting from the saturation coverage. All energetic data for CO dissociation are listed in Table 3 and the structures of initial states (IS), transition states (TS) and final states (FS) are given in the ESI.†

As discussed above, at n_{CO} = 10 (10/9 ML), the dissociation barrier (0.55 eV) of one 4F CO is close to the desorption energy (0.46 eV) of one top CO. However, CO dissociation is exothermic by 0.81 eV and more favored thermodynamically. The final state has 9CO + C + O co-adsorbed on the surface, and both C and O atoms are located at 4F sites.

Starting from 9CO + C + O, there are no free sites available for CO dissociation and the stepwise CO desorption energy is 0.49 and 0.50 eV, respectively. The final state has the co-adsorbed 7CO + C + O on the surface. Starting from 7CO + C + O, the CO desorption energy is lower than the corresponding dissociation barrier (0.51 *vs.* 0.71 eV), but CO dissociation is exothermic by 0.80 eV. Thermodynamically, the final state should have the co-adsorbed 6CO + 2C + 2O, which leads to further CO desorption (0.55 eV) since there are no free sites available for CO dissociation. The final state should have the co-adsorbed 5CO + 2C + 2O. It is noted that all the desorption energies of all CO molecules from 10CO to 6CO + 2C + 2O are very low (0.46–0.55 eV), and they are even slightly lower than the CO dissociation barriers (0.55–0.71 eV). This indicates the competitive desorption and dissociation of the adsorbed CO molecules and most importantly CO desorb at low temperature.

Starting from 5CO + 2C + 2O, the barrier of CO dissociation is much lower than the CO desorption energy (0.69 *vs.* 1.31 eV), and CO dissociation is exothermic by 0.50 eV. This leads to the formation of the co-adsorbed 4CO + 3C + 3O as the final state. Next is the stepwise CO desorption (1.30 and 1.53 eV, respectively) since there are no free sites available for CO dissociation. The final state is co-adsorbed 2CO + 3C + 3O.

Starting from 2CO + 3C + 3O, the barrier of CO dissociation is much lower than the CO desorption energy (0.89 *vs.* 1.70 eV), and CO dissociation is exothermic by 0.66 eV. This leads to the formation of the co-adsorbed 1CO + 4C + 4O as the final state, which has only CO desorption possibility (1.70 eV). The final state has the fully dissociatively adsorbed 4C + 4O.

On the basis of 4C + 4O, we computed the re-combinative CO stepwise desorption. It clearly shows the coverage dependent CO dissociative adsorption. For example, the re-combinative desorption energy gradually increases from 4C + 4O to 3C + 3O and 2C + 2O, as well as to 1C + 1O (3.12, 3.65, 3.66 and 3.97 eV, respectively).

It is now interesting to compare our results with the available experimental data. At first, the computed adsorption configurations along with their vibration frequencies are in agreement with the available experimental results. At low coverage, for example, CO prefers the tilted adsorption configurations at the 4F sites with very low vibration frequencies, whereas both tilted and atop configurations can co-exist at higher coverage with very low and high vibration frequencies. The very low CO frequencies come from the interaction of both C and O atoms with the surface Mo atoms.

Furthermore, it is found that the adsorbed CO molecules at the 4F sites can dissociate easily as long as free sites are available, and the dissociation barriers are practically coverage independent; the surface can have both molecular (α) and dissociative (β) adsorptions. This is in line with the observed CO dissociation at temperatures down to about 200 K as well as

Table 3 CO stepwise desorption energies (ΔE_{des}, eV), and dissociation barriers (E_a, eV) as well as dissociation energies (ΔE_{dis}, eV) at different coverage (# no free site available for CO dissociation)

ΔE_{des}	$CO(g) + (x-1)CO + yC + yO \leftarrow \mathbf{xCO + yC + yO} \rightarrow (x-1)CO + (y+1)C + (y+1)O$	E_a	ΔE_{dis}
0.46	$CO(g) + 9CO \leftarrow \mathbf{10CO} \rightarrow 9CO + 1C + 1O$	0.55	−0.81
0.49	$CO(g) + 8CO + 1C + 1O \leftarrow \mathbf{9CO + 1C + 1O} \rightarrow 8CO + 2C + 2O$	#	
0.50	$CO(g) + 7CO + 1C + 1O \leftarrow \mathbf{8CO + 1C + 1O} \rightarrow 7CO + 2C + 2O$	#	
0.51	$CO(g) + 6CO + 1C + 1O \leftarrow \mathbf{7CO + 1C + 1O} \rightarrow 6CO + 2C + 2O$	0.71	−0.80
0.55	$CO(g) + 5CO + 2C + 2O \leftarrow \mathbf{6CO + 2C + 2O} \rightarrow 5CO + 3C + 3O$	#	
1.31	$CO(g) + 4CO + 2C + 2O \leftarrow \mathbf{5CO + 2C + 2O} \rightarrow 4CO + 3C + 3O$	0.69	−0.50
1.30	$CO(g) + 3CO + 3C + 3O \leftarrow \mathbf{4CO + 3C + 3O} \rightarrow 3CO + 4C + 4O$	#	
1.53	$CO(g) + 2CO + 3C + 3O \leftarrow \mathbf{3CO + 3C + 3O} \rightarrow 2CO + 4C + 4O$	#	
1.70	$CO(g) + 1CO + 3C + 3O \leftarrow \mathbf{2CO + 3C + 3O} \rightarrow 1CO + 4C + 4O$	0.89	−0.66
1.70	$CO(g) + 4C + 4O \leftarrow \mathbf{1CO + 4C + 4O} \rightarrow 5C + 5O$	#	
3.12	$CO(g) + 3C + 3O \leftarrow \mathbf{4C + 4O}$		
3.65	$CO(g) + 2C + 2O \leftarrow \mathbf{3C + 3O}$		
3.66	$CO(g) + 1C + 1O \leftarrow \mathbf{2C + 2O}$		
3.97	$CO(g) \leftarrow \mathbf{1C + 1O}$		

the existence of molecular and dissociative co-adsorptions.[9] As shown in Table 3, the dissociated surface C and O atoms can hinder further CO dissociation due to the lack of free available sites for the dissociated C and O atoms.

On the basis of the computed data in Table 3, there are two groups of molecular CO desorptions: one with the desorption energy in the range of 0.46–0.55 eV and another one with the desorption energy in the range of 1.31–1.70 eV. Most importantly, there are three types of recombinative CO desorption: 3.12 eV for 4C + 4O, 3.65–3.66 eV for 3C + 3CO and 2C + 2O, and 3.97 eV for 1C + 1O. Indeed, this range of recombinative CO desorption energies (3.12–3.97 eV) is close to the estimated desorption activation energy as a function of coverage for the β states (2.9–3.7 eV),[9] as well as to the desorption energies in the range of 3.24–3.95 eV for a set of several binding states on polycrystalline molybdenum.[19] These ranges of energetic distribution are in agreement with the available TPD experiments. For example, Zaera *et al.*[12] reported five different binding states: two low-temperature (α) states with peak maxima at 150 and 290 K; and three high-temperature peaks at 840, 940 and 1250 K. In addition, Ko and Madix[10] reported a low-temperature state (α) with peak maxima at 330 K on the clean Mo(100) surface and 290 K on the Mo(100) surface saturated with dissociated (β) states as well as three β states at 900, 1024 and 1240 K.

4. Conclusion

Coverage dependent CO adsorption and dissociation on the Mo(100) surface were systematically calculated using the periodic density functional theory method. Structure optimization and CO frequency calculations were performed using the GGA-PBE method. For the discussion and comparison, single-point energies were acquired using the revised PBE method and the PBE-optimized structures.

It is found that CO prefers the 4-fold hollow site with tilted adsorption configuration at low coverage, as well as both tilted and atop adsorption configurations at high coverage. Tilted configurations are associated with very low C–O stretching frequencies and atop configurations are associated with high C–O stretching frequencies. These results are in full agreement with the experiment.

Within the entire range of CO coverage, CO dissociation has very low barriers and is exothermic as long as free sites are available; the barriers are nearly coverage independent. This nicely explains the experimentally observed CO dissociation at very low temperature. With the coverage increase, both molecular and dissociative adsorptions can coexist. The fact that the dissociated surface C and O atoms can hinder further CO dissociation is due to the lack of free available sites for the dissociated C and O atom rather than to the barriers.

On the basis of the computed competitive desorption and dissociative adsorption, there are two ranges of desorption energies: one for CO desorption from clean and up to 2C + 2O covered surface with coverage decrease and one for CO desorption from 2C + 2O to 4C + 4O covered surface with coverage decrease. It is most important to note that we also found three distinct desorption energies for CO recombinative desorption: one for 4C + 4O, one for 3C + 3O and 2C + 2O, and one for 1C + 1O. All these results are in full agreement with the results from the temperature-programmed desorption experiments.

Acknowledgements

This study was supported by the National Natural Science Foundation of China (no. U1510103).

References

1 R. B. Anderson, *The Fischer-Troposch Synthesis*, Academic Press, Orlando, FL, 1984; p. 3.
2 M. Saito and R. B. Anderson, *J. Catal.*, 1980, **63**, 438–446.
3 N. M. Schweitzer, J. A. Schaidle, O. K. Ezekoye, X. Q. Pan, S. Linic and L. T. Thompson, *J. Am. Chem. Soc.*, 2011, **133**, 2378–2381.
4 O. Korotkikh and R. Farrauto, *Catal. Today*, 2000, **62**, 249–254.
5 M. Bonn, S. Funk, Ch. Hess, D. N. Denzler, C. Stampfl, M. Scheffler, M. Wolf and G. Ertl, Phonon-Versus Electron-Mediated Desorption and Oxidation of CO on Ru(0001), *Science*, 1999, **285**, 1042–1045.
6 S. Zaman and K. J. Smith, *A Catal. Rev.*, 2012, **54**, 41–132.
7 J. Lecante, R. Riwan and C. Guillot, *Surf. Sci.*, 1973, **35**, 271–287.
8 C. Guillot, R. Riwan and J. Lecante, *Surf. Sci.*, 1976, **59**, 581–592.
9 T. E. Felter and P. J. Estrup, *Surf. Sci.*, 1978, **76**, 464–482.
10 E. I. Ko and R. J. Madix, *Surf. Sci.*, 1980, **100**, L505–L509.
11 E. I. Ko and R. J. Madix, *Surf. Sci.*, 1981, **109**, 221–238.
12 F. Zaera, E. Kollin and J. L. Gland, *Chem. Phys. Lett.*, 1985, **121**, 464–468.
13 J. P. Fulmer, F. Zaera and W. T. Tysoe, *J. Chem. Phys.*, 1987, **87**, 7265–7271.
14 A. G. Jackson and M. P. Hooker, *Surf. Sci.*, 1967, **6**, 297–308.
15 J. W. Ericson and P. J. Estrup, *Surf. Sci.*, 1986, **167**, 519–533.
16 J. G. Chen, M. L. Colaianni, W. H. Weinberg and J. T. Yates Jr., *Chem. Phys. Lett.*, 1991, **177**, 113–117.
17 J. W. He, W. K. Kuhn and D. W. Goodman, *Surf. Sci.*, 1992, **262**, 351–358.
18 A. J. Jaworowskia, M. Smedha, M. Borga, A. Sandellb, A. Beutlera, S. L. Sorensena, E. Lundgrena and J. N. Andersena, *Surf. Sci.*, 2001, **492**, 185–194.
19 A. D. Crowell and L. D. Matthews, *Surf. Sci.*, 1967, **7**, 79–89.
20 P. Liu and J. A. Rodriguez, *Catal. Lett.*, 2003, **91**, 247–252.
21 Z. Ji and J. Q. Li, *J. Phys. Chem. B*, 2006, **110**, 18363–18367.
22 F. J. E. Scheijen, J. W. Niemantsverdriet and D. C. Ferre, *J. Phys. Chem. C*, 2007, **111**, 13473–13480.
23 F. J. E. Scheijen, D. C. Ferre and J. W. Niemantsverdriet, *J. Phys. Chem. C*, 2009, **113**, 11041–11049.
24 N. V. Petrova, *J. Phys. Chem. Solids*, 2011, **72**, 744–748.
25 G. Kresse and J. Furthmüller, *Comput. Mater. Sci.*, 1996, **6**, 15–50.
26 G. Kresse and J. Furthmüller, *Phys. Rev. B: Condens. Matter Mater. Phys.*, 1996, **54**, 11169–11186.

27 P. E. Blochl, *Phys. Rev. B: Condens. Matter Mater. Phys.*, 1994, **50**, 17953–17979.
28 G. Kresse, *Phys. Rev. B: Condens. Matter Mater. Phys.*, 1999, **59**, 1758–1775.
29 J. P. Perdew, K. Burke and M. Ernzerhof, *Phys. Rev. Lett.*, 1996, **77**, 3865–3868.
30 M. Methfessel and A. T. Paxton, *Phys. Rev. B: Condens. Matter Mater. Phys.*, 1989, **40**, 3616–3621.
31 G. Henkelman and H. Jónsson, *J. Chem. Phys.*, 2000, **113**, 9978–9985.
32 B. Hammer, L. B. Hansen and J. K. Norskov, *Phys. Rev. B: Condens. Matter Mater. Phys.*, 1999, **59**, 7413.
33 E. R. McNellis, J. Meyer and K. Reuter, *Phys. Rev. B: Condens. Matter Mater. Phys.*, 2009, **80**, 205414.
34 D. L. Chen, W. A. A. Saidi and J. K. Johnson, *J. Phys.: Condens. Matter*, 2012, **24**, 424211.
35 T. Bučko, J. Hafner, S. Lebègue and J. G. Ángyán, *J. Phys. Chem. A*, 2012, **114**, 11814–11824.
36 P. Zhao, Y. R. He, D.-B. Cao, X. D. Wen, H. W. Xiang, Y.-W. Li, J. Wang and H. Jiao, *Phys. Chem. Chem. Phys.*, 2015, **17**, 19446–19456.
37 S. L. Liu, X. X. Tian, T. Wang, X. D. Wen, Y.-W. Li, J. Wang and H. Jiao, *J. Phys. Chem. C*, 2014, **118**, 26139–26154.
38 S. L. Liu, X. X. Tian, T. Wang, X. D. Wen, Y.-W. Li, J. Wang and H. Jiao, *Phys. Chem. Chem. Phys.*, 2015, **17**, 8811–8821.
39 S. L. Liu, X. X. Tian, T. Wang, X. D. Wen, Y.-W. Li, J. Wang and H. Jiao, *J. Phys. Chem. C*, 2015, **119**, 11714–11724.
40 T. Wang, X. X. Tian, Y.-W. Li, J. Wang, M. Beller and H. Jiao, *J. Phys. Chem. C*, 2014, **118**, 1095–1101.
41 T. Wang, X. X. Tian, Y.-W. Li, J. Wang, M. Beller and H. Jiao, *ACS Catal.*, 2014, **4**, 1991–2005.
42 X. X. Tian, T. Wang, Y. Yang, Y.-W. Li, J. Wang and H. Jiao, *Appl. Catal., A*, 2017, **530**, 83–92.
43 S. Liu, Y.-W. Li, J. Wang and H. Jiao, *Catal. Sci. Technol.*, 2016, **6**, 8336–8343.
44 T. Wang, Y.-W. Li, J. Wang, M. Beller and H. Jiao, *J. Phys. Chem. C*, 2014, **118**, 3162–3171.
45 T. Wang, Q. Q. Luo, Y.-W. Li, J. Wang, M. Beller and H. Jiao, *Appl. Catal., A*, 2014, **478**, 146–156.
46 R. V. Belosudov, S. Sakahara, K. Yajima, S. Takami, M. Kubo and A. Miyamoto, *Appl. Surf. Sci.*, 2002, **189**, 245–252.